



Numerical and analytical analysis of a monopile-supported offshore wind turbine under ship impacts



Ming Song ^a, Zhiyu Jiang ^{b,*}, Wei Yuan ^c

^a School of Naval Architecture and Ocean Engineering, Jiangsu University of Science and Technology, Zhengjiang, 212003, China

^b Department of Engineering Sciences, University of Agder, N-4898, Grimstad, Norway

^c Graduate School, Jiangsu University of Science and Technology, Zhengjiang, 212003, China

ARTICLE INFO

Article history:

Received 25 August 2020

Received in revised form

2 November 2020

Accepted 18 November 2020

Available online 25 November 2020

Keywords:

Offshore wind turbine

Ship collision

Wind load effect

Dynamic response

Analytical model

Accidental limit state

ABSTRACT

Offshore wind turbines in the vicinity of ship traffic are exposed to increased risks of ship collisions. To better understand the impact mechanism, this paper evaluates the dynamic responses of a monopile-supported wind turbine under ship impacts, using both numerical and analytical methods. The nonlinear finite element method is applied during the numerical simulations, and the wind load effects, soil conditions, and rigid and deformable ship bows are considered. The analytical approach, originally developed based on the energy method, is extended here to address the damping effects of monopile-supported wind turbines. In the case study, the impacts are studied between a 4600-ton vessel and a 5-MW offshore wind turbine. The effects are presented of the aerodynamic damping, ship impact velocity, mean wind speed, wind direction, and ship bow stiffness on the collision responses. A comparison between the numerical and analytical results shows a generally good agreement for the maximum contact force. Under an impact velocity of 1 m/s and 3 m/s, the discrepancy between the two methods is 5% and 7%, respectively. The developed engineering approaches can be used to address accidental collision problems between ships and bottom-fixed offshore wind turbines.

© 2020 The Author(s). Published by Elsevier Ltd. This is an open access article under the CC BY license (<http://creativecommons.org/licenses/by/4.0/>).

1. Introduction

Offshore wind energy is an attractive form of renewable energy resources. Since 1990s, the offshore wind industry has been expanding successfully. The global offshore wind power installation reached a capacity of 19 GW by 2017 [1]. Today, offshore wind farms have been constructed across more than 10 European countries. The average water depth of those offshore wind farms is close to 30 m and most offshore wind turbines (OWTs) are supported by monopile foundations [2].

The design of modern OWTs is primarily based on a semi-probabilistic approach [3] focusing on the design load cases related to extreme environmental conditions [4,5] or fault conditions [6]. Accidental events like ship collisions are not yet addressed in practice, probably due to the marginal profitability of the offshore wind energy sector and the low occurrence rate of such events. Still, as an increasing number of offshore wind farms are located close to ship traffic routes, the risks of collisions between

ships and OWTs increase [7]. During an accidental ship impact, the consequence of structural failures of an unmanned OWT is normally lower compared to that of a ship, as ship damages can lead to capsizing, or in the worst case, loss of human lives. Moreover, dropped objects of the damaged OWT can also pose threat to ship safety. Although these scenarios are not fully understood because of the complex dynamic interactions between a ship and an OWT during a collision, the collision loads from ships are very important for the structural design of OWTs.

There are design standards, e.g., NORSOK [8], BSH [9] and IEC [10], which provide guidance on how to design OWTs to resist the ship collision-induced impact forces. According to DNVGL-ST-0437 [11], the primary structure, boat landings and other secondary structures in and near the waterline are required to be designed for supply vessel impacts as a normal event, in which the vessel speed shall not be less than 0.5 m/s and the effects of hydrodynamic added mass shall be included. Additionally, these primary structures are required to be designed for impacts as an abnormal event, in which the vessel speed shall not be less than 2.0 m/s. However, no specific ship size and impact energy requirement is given by the standard. Compared to the DNVGL standard, the NORSOK N-004

* Corresponding author.

E-mail addresses: zhiyu.jiang@uia.no, zhiyu.jiang1896@gmail.com (Z. Jiang).

Standard [8] presents force-deformation relationships for multiple collision scenarios of a supply vessel with a displacement of 5000 tons colliding with an infinite rigid vertical cylinder of various diameters.

Simplified analytical methods are useful tools to assess the energy dissipation of collisions between ships and offshore structures and have been developed by researchers in the past. Buldgen et al. [12] presented a simplified analytical method for estimating the crushing resistance of an oblique cylinder impacted by the stem of a striking ship. Pire et al. [13] developed analytical formulations to assess the energy dissipated plastically at the base of an offshore jacket structure impacted by a ship. Analytical procedures were presented for analysis of the external dynamics of ship collisions against bottom-supported offshore structures; see Pedersen and Jensen [14], Pedersen and Zhang [15], and Pedersen [16]. In these works, algebraic expressions were derived for the maximum values of collision forces and energy released for local crushing on basis of the principles of conservation of momentum and energy. However, there exist several limitations for the simplified analytical method as we cannot use it to estimate detailed collision behaviors including time histories of the collision force, energy dissipation, tower motion or structural damage. Numerical analysis, on the other hand, provides a means to achieve a better understanding of the collision damage and of the responses of an OWT at the expense of increased computational resources.

A few researchers have studied the numerical analysis of ship-OWT collisions [17–19]. Impact simulations between a jacket-supported OWT and a large oil tanker were carried out by Ramberg [20] who considered the high impact energy, assumed a rigid ship, and represented the contact between the structures by a nonlinear spring. Moulas et al. [21] carried out the collision simulation of vessels with two common types of fixed-bottom foundations, namely the monopile and the jacket support structures. In a work by Hao and Liu [22], a comparison of the foundations' damage and OWTs' response was made for head-on collisions between low-energy ships and OWTs, and three types of foundations were considered including the monopile, the tripod, and the jacket support structures. Bela et al. [23] investigated the influence of impact velocity, impact location, wind loads and boundary conditions on the behavior of an OWT with a monopile support subjected to the impact of a rigid ship. However, the wind loads were assumed to be constant during the simulation, which is an oversimplification.

Despite the aforementioned studies, to the authors knowledge, no work has addressed the interaction between wind loads and OWT response in the analysis of ship-OWT collisions. In reality, for an OWT, wind loads are the primary external loads, which cause the tower to oscillate before the actual impact and affect the motion of an OWT after the impact. On the other hand, the OWT motions may also have an influence on the wind loads. Therefore, it is necessary to take into account the interaction between the wind loads and the wind turbine motions when dealing with the dynamic responses of an OWT under a ship impact.

To obtain more accurate response evaluation of a monopile-supported OWT subjected to ship impact, this paper considers the interaction between the wind loads and the motion of OWT in the dynamic analysis. To the authors' knowledge, this is the first attempt to consider this interaction for ship-OWT collision problems. Numerical simulations of a head-on collision between a 4600-ton vessel and the NREL 5-MW OWT (OC3 Phase II monopile) are carried out by LS-DYNA [24]. The effects of various parameters on collision response are investigated. In addition, a simplified analytical approach is extended to calculate the maximum collision force, the energy dissipation, and the maximum tower-top displacement. These results are compared with those obtained by

the numerical method.

The layout of the paper is arranged as follows. Section 2 describes the problem statement of the ship-OWT monopile collision scenario. Section 3 presents numerical modeling of the ship-OWT collision. Section 4 presents details of the simplified analytical approach. Section 5 describes the details of the case study, including the striking ship and the monopile-supported OWT models and load cases. Results and discussions are presented in Section 6, and finally, conclusions are presented in Section 7.

2. Problem statement

The impact angle between a ship and an OWT with a monopile foundation is arbitrary in an accident, in which a head-on impact causes the highest reaction force. If the OWT collapses due to a large impact force and the wind turbine components fall onto the ship, this scenario can lead to serious damage of the ship and may cause human deaths or injuries. Therefore, all collision scenarios assume a head-on impact in this paper.

When a ship impacts an OWT, the operational conditions (operational or parked) of the wind turbine depends on the wind speed. The free wind speed also affects the magnitudes of wind loads acting on the turbine. Hence, various collision scenarios with the mean wind speed varying from 0 m/s to 30 m/s are selected. Besides, the direction of wind speed relative to the ship impact angle is arbitrary. Here, we consider three directions, i.e., 0°, 90°, 180°, which are shown in Fig. 1. It is assumed that the wind turbine has an active yaw system and the rotor plane is always perpendicular to the main wind direction.

3. Numerical modeling

3.1. Structural modeling

The nonlinear finite element method based on explicit time integration [24] is used here for analyzing the dynamic response of structures. The discrete equations of motion at time instant t^n are:

$$Ma^n = P^n - F^n + H^n \tag{1}$$

where M is the diagonal mass matrix including both the monopile and the ship, a^n is the acceleration vector, P^n accounts for external and body force loads, F^n is the stress divergence vector, and H^n is the hourglass resistance. The primary nonlinearities, which are due to geometric effects, inelastic material behavior and contact behavior, are accounted for in F . Additional nonlinearities arise in P due to geometry dependent applied loads. To advance to time t^{n+1} , the central difference time integration is used:

$$a^n = M^{-1}(P^n - F^n + H^n) \tag{2}$$

$$v^{n+1/2} = v^{n-1/2} + a^n \Delta t \tag{3}$$

$$u^{n+1} = u^n + v^{n+1/2} \Delta t \tag{4}$$

$$nt^{n+1/2} = \frac{(nt^n + nt^{n+1})}{2} \tag{5}$$

where v and u are the global nodal velocity and displacement vectors, respectively. The geometry is updated by adding the displacement increments to the initial geometry:

$$x^{n+1} = x^0 + u^{n+1} \tag{6}$$

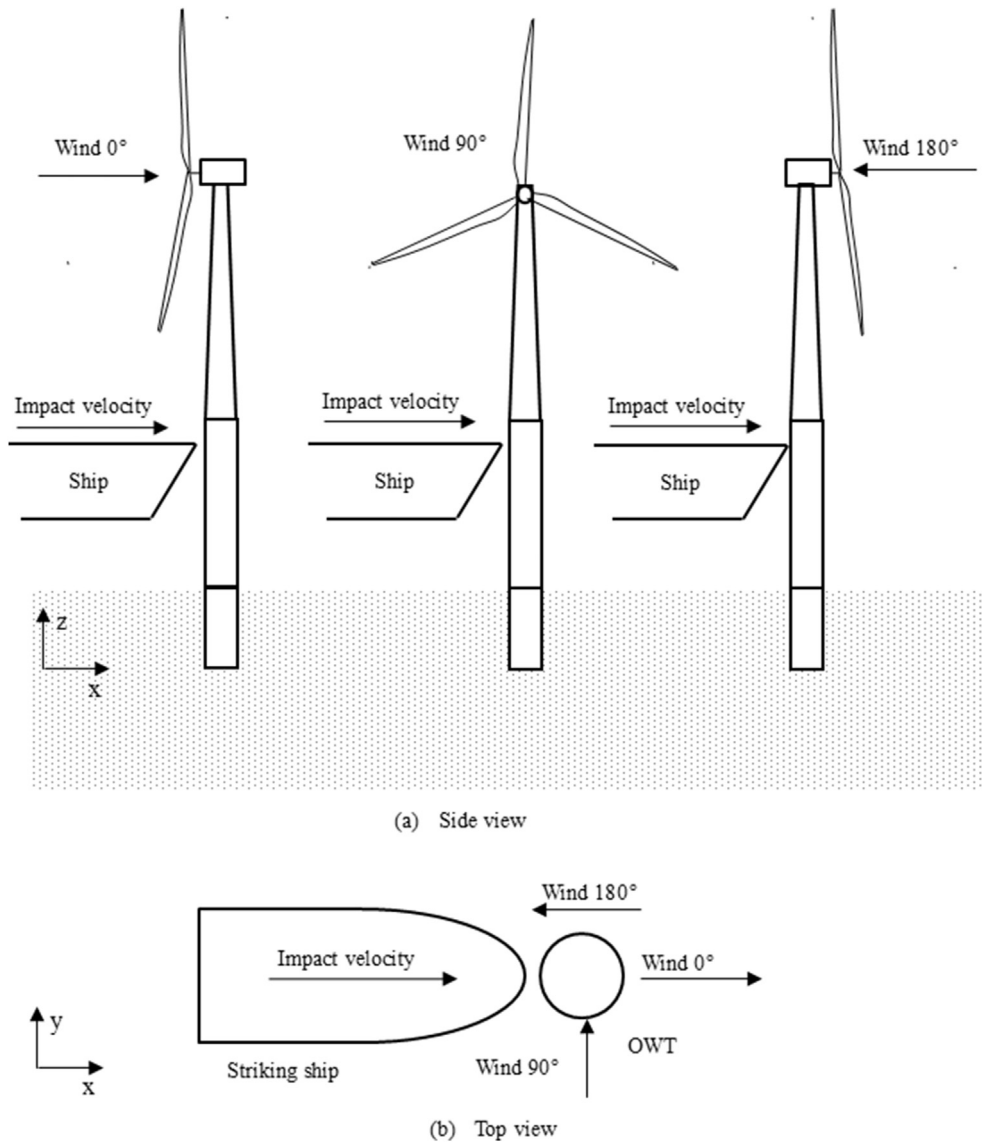


Fig. 1. Direction of wind speed (Wind 0°: wind speed has the same direction as the impact velocity; Wind 90°: wind speed is perpendicular to the impact velocity; Wind 180°: wind speed and impact velocity have opposite directions).

The finite element models of a ship and a monopile OWT are modeled using Patran [25]. In order to simplify the modeling, the nacelle and rotor blades of the wind turbine are replaced by a lumped mass located at the top of the tower. The connection between the tower and the transition piece is assumed to be rigid. As the natural frequencies of an OWT affect the structure’s dynamic behavior, a modal analysis must be performed for the simplified OWT model. The damping ratio of 1% critical damping factor for the lowest frequency mode is assumed for the OWT in the ship-OWT collision simulations. This damping ratio level is consistent with those specified for the structural components of the NREL 5-MW OWT.

The numerical analysis of collision between a ship and an OWT monopile is conducted using LS-DYNA. To consider the interaction between the soil and the monopile, the distributed springs model is used which idealizes the seabed contact with a flexible foundation. The subsoil spring stiffness constants are depth-dependent and are calculated based on a linearization of the p - y model. Two spring elements in the x - and y -directions (Fig. 1) are applied at different

depths of piles. Each spring has two end nodes in which one node is linked to the pile and the other node is fixed in all directions. The bottom of the pile is fixed in translation in the z -direction and constrained from rotation about the z -axis.

An elastic-plastic material model with the power-law hardening is used for the deformable ship bow and the OWT. The material’s stress-strain constitutive relation is given as follows:

$$\sigma = k(\epsilon_{yp} + \bar{\epsilon}^p)^n \tag{7}$$

$$\epsilon_{yp} = \left(\frac{\sigma_y}{k}\right)^{\frac{1}{n}} \tag{8}$$

where σ_y is the yield stress, ϵ_{yp} is the elastic strain to yield, $\bar{\epsilon}^p$ is the effective plastic strain, k is the strength coefficient and n is the hardening exponent.

3.2. Modeling of the wind load effect

During a ship collision, the tower top of a fixed-bottom OWT may experience violent vibrations during the first few seconds. For an operating wind turbine, such vibrations are expected to induce a sudden change in the relative inflow wind speed and to affect the aerodynamic loads and dynamic responses of the OWT consequently, depending on the severity of the ship impact. As previous researches [17] largely ignored this aspect during the numerical simulations, the influence of the wind loads on the impact-induced dynamic responses is not clear.

To consider the wind load effect on an operating OWT, modeling approaches on different fidelity levels exist depending on the purpose of the analysis. The high-fidelity approaches apply the computational fluid dynamics methods to discretize the Navier-Stokes equations in order to obtain accurate rotor aerodynamics and the corresponding computational costs are also very high [26]. On the other hand, engineering approaches based on the classical blade element momentum method [27] have been widely adopted by aeroelastic codes, e.g., FAST [28] and HAWC2 [29]. One key step of the blade element momentum method is to determine induced velocities at the rotor plane by assuming equilibrium between the applied aerodynamic loads and the induced flow field. After being modified by features like dynamic inflow or dynamic stall, the engineering approaches can reliably predict OWT responses in various operational conditions. However, as the analysis purpose is to assess the global motions and structural responses of OWTs, the wind turbine structures including support structures and blades are often modeled as beam elements and the control actions must be considered.

The last modeling approach regards the wind excitation as an independent phenomenon from wave excitations and incorporates the wind load effect as a damping source termed as “aerodynamic damping”. Consider a tower-top in motion. When the tower-top is moving forward, the rotor experiences a small increase in the relative wind speed and in the thrust which will counteract the tower-top motion [30]. Analogously, when the tower top moves backward, the thrust decreases and hinders the motion in that direction. This effect is considered a damping because it relates to the velocity-proportional term in the equation of motion. The idea of aerodynamic damping was originally proposed by Kühn [31] and further developed by Tempel [32] and Salzmann [30]. This modeling approach, albeit simplified, does not require finite element modeling of wind turbine blades or determination of rotor aerodynamics in the time domain, thus allowing an efficient assessment of fixed-bottom and floating support structures; see Ref. [33]. For ship-OWT collision analysis, the focus will be on structural responses of wind turbine support structures and ship structures which involve a large number of finite elements. Therefore, we adopt the last modeling approach and represent the wind load effect by considering the aerodynamic damping in addition to the mean thrust force.

There are different methods for estimating the aerodynamic damping of a variable-speed wind turbine in operation [30]. As suggested in Refs. [34], the linearized aerodynamic damping can be numerically estimated based on changes in the thrust force due to a change in wind speed without considering the effect of the control system:

$$c_{aero} = \frac{dF_{Thrust}}{dV_{mean}} \quad (9)$$

where dV_{mean} denotes a small variation in the mean wind speed and dF_{Thrust} denotes the corresponding change in the thrust force. For a range of constant wind speeds, time-domain simulations were

carried out in an aeroelastic code for a land-based wind turbine with the blade pitch and rotor speed fixed for each wind speed, and the damping values are estimated accordingly. Note that Eq. (9) is only valid for operating wind turbines. For parked (standing-still or idling) wind turbines, the mean wind loads and the aerodynamic damping are deemed small.

As mentioned above, the numerical collision analysis is performed in LS-DYNA in the time domain, and the coupling between the main program and the simplified aerodynamic model is made by the user-defined load subroutine LOADSETUD which provides a means to apply nodal loads as a function of velocity. The architecture of the coupling algorithm is shown in Fig. 2. First, the wind loads and the aerodynamic damping c_{aero} for the mean wind speed are precalculated using the HAWC2 code. The aerodynamic damping includes the effect of wind shear across the rotor plane, and a constant power law exponent of 0.14 is used for OWTs [10]. During the time-domain simulation, only constant wind speed is considered, and the mean wind loads are applied on the tower-top node. The wind drag loads on the tower are not considered as they are negligible. At each time step, LS-DYNA passes information of the velocity of the tower-top node to the user subroutine. The nodal velocity history is stored, and the aerodynamic damping force equivalent to $c_{aero} * V_{vib}$ is calculated in the user load subroutine. Here, c_{aero} is the precalculated damping coefficient and V_{vib} is the vibration-induced velocity of the tower-top node. It is expected that V_{vib} increases immediately after the ship impact and reduces to zero eventually. The obtained aerodynamic damping load is applied on the tower top node, and LS-DYNA then calculates the structural deformation and tower motion, and provides information of the tower-top motion for the next time step.

4. Simplified analytical approach

A simplified analytical approach is used here to estimate the collision results. The response of the OWT is assumed to be a linear summation of the deflections due to wind load and collision force separately. This simplified approach cannot consider the interaction between the wind load and the collision force. Neither can this method address the soil conditions or predict the collapse of the OWT.

The deflection of the tower top under wind loads is calculated based on the beam theory where the OWT is assumed as a cantilever beam of variable cross-section. The simplified OWT structure is shown in Fig. 3. Here, section AB represents the tower with various cross-section and section BC represents the transition piece and the monopile with a constant cross-section. The deflection should be calculated in sections due to the varying cross-section areas and wall thicknesses.

For section AB with variable cross sections (Fig. 3), the deflection of the tower-top point, A, is given by

$$u_1 = \frac{F_w}{Ewtk^3} (A_1 + A_2) \quad (10)$$

$$A_1 = \frac{L_s}{L_z} - 1 + \ln L_z \quad (11)$$

$$A_2 = \frac{L_s}{2} \left(\frac{2}{L_z} - \frac{1}{L_s} - \frac{L_s}{L_z^2} \right) \quad (12)$$

where F_w is the wind load, E is the elastic modulus, $k = (D_z - D_s)/L_z$, D_z is the diameter of the tower base, D_s is the diameter of the tower-top, L_z is the height of the tower $L_s = D_s/k$, $L_z = L_s + L_2$, t is the average wall thickness, and w is the coefficient of inertia

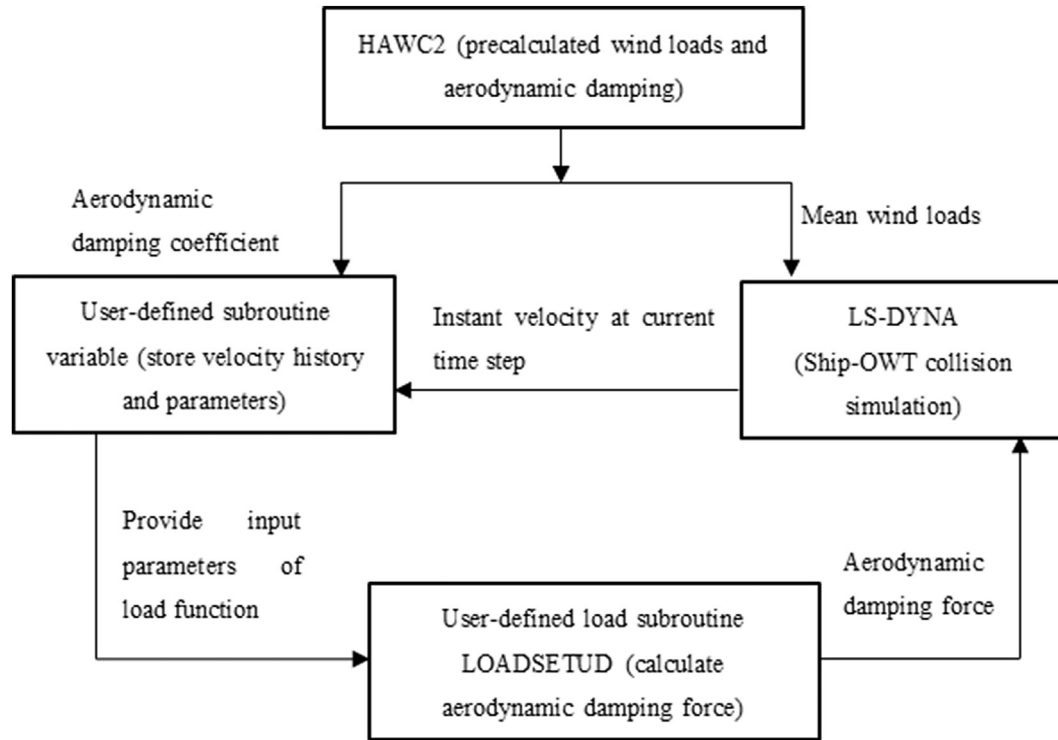


Fig. 2. Flowchart of the coupling algorithm for the numerical simulation in LS-DYNA.

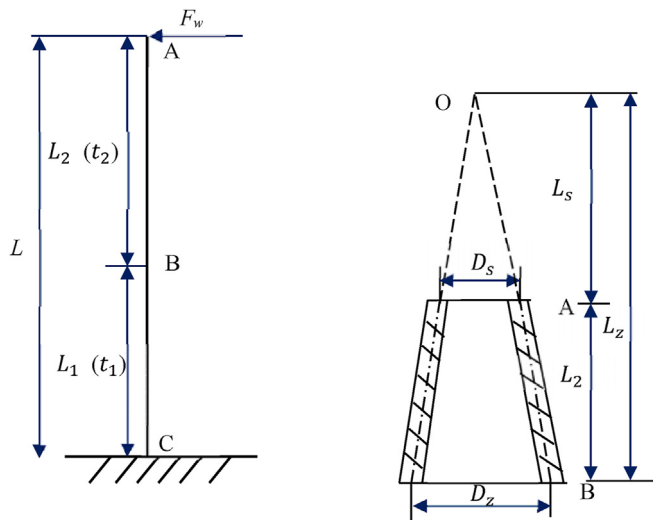


Fig. 3. Schematic of a simplified OWT structure.

$$u_2 = \frac{F_B L_1^3}{3EI} = \frac{F_w L_1^3}{3EI} \tag{15}$$

$$\theta_2 = \frac{F_B L_1^2}{2EI} = \frac{F_w L_1^2}{2EI} \tag{16}$$

$$u_3 = \frac{M_B L_1^2}{2EI} = \frac{F_w L_2 L_1^2}{2EI} \tag{17}$$

$$\theta_3 = \frac{M_B L_1}{EI} = \frac{F_w L_2 L_1}{EI} \tag{18}$$

where L_1 is the total height of the transition piece and the monopile and I is the second moment of area of the cross section.

The deflection of the tower top under the wind load can be obtained as

$$u_A = u_1 + u_2 + u_3 + (\theta_2 + \theta_3)L_2 \tag{19}$$

moment which equals 0.393 for circular cross section [35].

For section BC with constant cross sections, the force and the bending moment acting on point B are

$$F_B = F_w \tag{13}$$

$$M_B = F_w L_2 \tag{14}$$

Then, the deflection and rotation angle at point B under F_B and M_B can be calculated accordingly, and we obtain the following expressions

The collision force, the energy dissipation, and the deflection of the tower top subjected to ship impact are calculated based on the principles of conservation of momentum and conservation of energy. The simple algebraic expressions proposed by Pedersen are developed here with consideration of the damping effect. For details, refer to Pedersen and Jensen [14], Pedersen and Zhang [15], and Pedersen [16].

The analysis system can be approximated as a two-mass system in which one mass m_s represents the mass of the ship and its added mass, and the other mass, m_t , represents the generalized mass of the OWT structure. The simplified 2-D impact model is shown in Fig. 4. Hence, the impact behavior of the wind turbine structure can be represented by the following elastic stiffness relations:

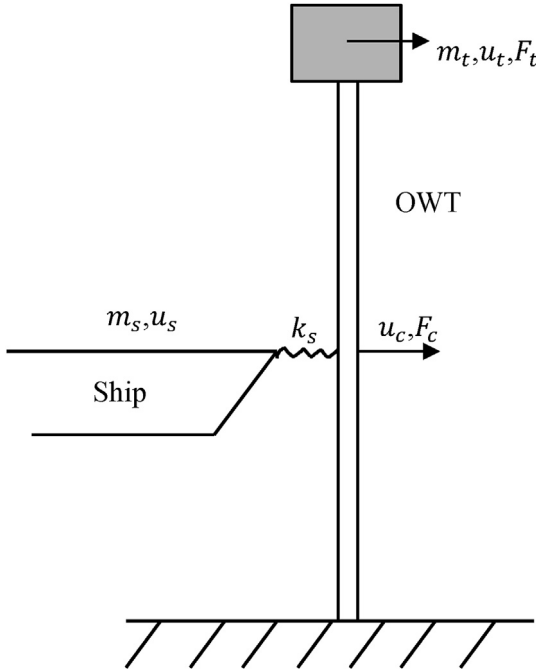


Fig. 4. Simplified model of ship impact on OWT.

$$F_c = k_{11}u_c + k_{12}u_t \quad (20)$$

$$F_t = k_{21}u_c + k_{22}u_t = -m_t\ddot{u}_t + c_t\dot{u}_t \quad (21)$$

where k_{ij} is the generalized stiffness coefficients with subscripts i and j , F_c is the internal collision force, F_t is the internal transmitted force acting on the generalized topside mass m_t , u_c is the displacement of the collision point, u_t is the displacement of the topside, c_t is the linear damping term including structural damping (Rayleigh damping), radiation damping of the support structure, soil damping, and aerodynamic damping, and \dot{u}_t is the velocity of the topside.

The interaction between the ship and the wind turbine can be approximated by the following simple relation

$$F_c = \begin{cases} nk_s(u_s - u_c) & \text{for } \dot{u}_s - \dot{u}_c \geq 0 \\ 0 & \text{for } \dot{u}_s - \dot{u}_c < 0 \end{cases} \quad (22)$$

where k_s is a stiffness coefficient, and u_s is the displacement at the collision point of the ship.

The maximum value of the collision force at the end of the first crushing phase is reached when the velocity of the ship \dot{u}_s equals the velocity of the contact point \dot{u}_c . From Equation (20), we get

$$\dot{u}_s = -\frac{k_{12}}{k_{11}} \dot{u}_t \quad (23)$$

The displacement u_t of the wind turbine mass is assumed to be small during the first crushing phase. Thus, the generalized force F_t can be approximated by

$$F_t = -\frac{k_{21}}{k_{11}} F_c \quad (24)$$

The conservation of momentum can be expressed as

$$I_c = m_s(V_0 - \dot{u}_s) = \int_0^{t_1} F_c(t) dt \quad (25)$$

$$I_t = -m_t\dot{u}_t = \int_0^{t_1} (F_t(t) - c_t\dot{u}_t) dt = \int_0^{t_1} F_t(t) dt - c_t u_t \approx \int_0^{t_1} F_t(t) dt \quad (26)$$

where t_1 denotes the duration of the first phase. From Equations 23–26, the velocity \dot{u}_t of the center of gravity of the topside structure at the time of maximum collision force, F_c , is found below:

$$\dot{u}_t = \frac{-V_0}{\frac{k_{12}}{k_{11}} + \frac{k_{11}}{k_{21}} \frac{m_t}{m_s}} \quad (27)$$

At the end of the first phase, the displacement of the topside u_t is assumed to be small, and consequently the damping energy can be neglected. Based on energy conservation, the following relation holds:

$$\frac{1}{2}m_s V_0^2 = \frac{1}{2}k_c u_s^2 + \frac{1}{2}m_s \dot{u}_s^2 + \frac{1}{2}m_t \dot{u}_t^2 \quad (28)$$

where $k_c = \frac{k_{11}k_s}{k_{11}+k_s}$ is the stiffness seen from the ship for zero deflection of the wind turbine mass.

The maximum collision force at the end of first phase is found as

$$F_c = k_c u_s \quad (29)$$

The deformation energy which is absorbed as plastic deformation during the first phase can be expressed as

$$E_{ship} = \frac{1}{2}F_c(u_s - u_c) = \frac{F_c^2}{2k_s} \quad (30)$$

At the end of the second phase of the collision, all energies except the absorbed plastic deformation energy are assumed to exist in the forms of deformation energy and damping energy. That is

$$\frac{1}{2}m_s V_0^2 - E_{ship} = \frac{1}{2}(F_t u_t + F_c u_c) + \int_{t_1}^{t_2} c_t \dot{u}_t du_t \quad (31)$$

At the end of second phase ($t = t_2$), the collision force F_c is considered small, and the energy distribution due to this force can be neglected, i.e., $F_c u_c \approx 0$. We further assume that the damping force (i.e. $c_t \dot{u}_t$)-displacement relationship is linear during this phase, so this expression can be rewritten as

$$\frac{1}{2}m_s V_0^2 - E_{ship} = \frac{1}{2}F_t u_t + \int_{t_1}^{t_2} c_t \dot{u}_t du_t = \frac{1}{2}k_p (u_t)^2 + \frac{1}{2}c_t u_t u_t \quad (32)$$

Hence, the deflection of the tower top under the collision force can be approximated by

$$u_t = \frac{-c_t \dot{u}_t + \sqrt{(c_t \dot{u}_t)^2 + 4k_p (m_s V_0^2 - 2E_{ship})}}{2k_p} \quad (33)$$

where $k_p = \frac{k_{11}k_{22} - k_{12}^2}{k_{11}}$ is the generalized stiffness of the unconstrained topside center of gravity.

Finally, the deflection of the tower top subjected to the wind load and the impact load is found as

$$u_{total} = u_A + u_t \tag{34}$$

5. Case study

We consider the above-described collision in a case study where a 4600-ton displacement multipurpose vessel impacts the NREL 5-MW OWT supported by a monopile foundation [36]. In fact, any ships can pose collision risks to OWTs, and the selected vessel is just representative of a certain class considering the NORSOK N-004 standard [8]. The principal dimensions of the ship are listed in Table 1. The surge added mass of the vessel is assumed to be 25% of the displacement for bow collision [11].

The main area in the ship bow is meshed with shell elements with a size of approximately 150 mm, in which the element-length-to-thickness ratio is within the range of 5–10 such that the local stress and strain fields can be well captured [37]. The remaining part of the vessel is meshed with rigid shell elements with a size of 600 mm. The total number of the elements for the ship is 66,053. The finite element model of the vessel is illustrated in Fig. 5.

The NREL 5-MW OWT has a height of 143.6 m and a rotor-nacelle assembly mass of 350 t. The structure consists of a monopile, a transition piece, and a tower. The monopile and the transition piece have a constant cross section with an outer diameter of 6.0 m and a wall thickness of 60 mm. There are 36 m of the monopile driven into the soil. The tower has a height of 77.6 m with a base diameter of 6 m and a top diameter of 3.87 m. The wall thickness decreases from 27.0 mm near the bottom to 19.4 mm in the upper region. The cut-in, rated and cut-out wind speeds for the variable-speed pitch-regulated wind turbine are 3 m/s, 11.4 m/s, and 25 m/s, respectively.

All structures are modeled with the Belytchko-Tsay shell element with five integration points over the thickness. A fine mesh with a size of 200 mm is applied to the contact area and to the top of the structure, and a coarse mesh size of 500 mm is used for the rest of the wind turbine structure (Fig. 6). The numerical OWT model consists of 29,768 shell elements.

The steel's material parameters used for the deformable ship bow and the OWT are listed in Table 2. It is noted that the effective density of the OWT is taken to be 8500 kg/m³ to account for paint, bolts, welds and flanges that are not considered in the wall thickness data.

In total, 36 collision cases are simulated; see Table 3. The ship bow is assumed to be rigid in the first 33 cases to evaluate the effects of various parameters assumed in Le Sourne et al. [19] and Bela et al. [23]. In the last 3 cases, in order to consider the energy dissipated by the ship, a deformable bow is used. In cases 7–9, 16–24 and 34–36, the rated wind speed of 11.4 m/s is selected because the corresponding wind-induced thrust forces are largest. Three wind directions (0°, 90°, 180°; see Fig. 1) and three impact velocities (1 m/s, 2 m/s and 3 m/s) are selected in cases 1–24 to

Table 1
List of the main dimensions of the multipurpose vessel.

Length overall (m)	98.5
Breadth (m)	17.0
Depth (m)	8.8
Draft (m)	6.0
Displacement (ton)	4600
Second deck to upper deck distance (m)	2.65
Transverse bulkhead-1 to contact point distance (m)	12.05

investigate the effect of the wind direction and the impact velocity. The aerodynamic damping is not considered in cases 1–9 but is considered in cases 10–18. To study the effect of the wind speed, wind speeds varying from 0 to 30 m/s are selected in cases 25–33. The wind turbine is parked when the wind speed is below 5 m/s or above 25 m/s, and the condition of the wind turbine is given in Table 3. In all simulations, the friction coefficient between the ship bow and the OWT is set to 0.3, and the same friction coefficient is applied to the internal structure contacts.

6. Results and discussions

6.1. Verification of the simplified OWT

The natural frequencies of an OWT influence the structure's dynamic behavior under ship impacts. For the present investigation, the focus is on the OWT's global response and structural deformation of the support structure. Hence, we only compare the lowest natural frequencies of the simplified OWT against the those of the system with a full rotor. The modal analysis of the simplified OWT is carried out by Patran. The calculated natural frequencies of the lowest eigenmodes in the fore-aft and side-side directions are approximately 0.24 Hz. These results match those of the full system predicted by the HAWC2 code, which indicates that the simplified OWT model can reflect the structure dynamic behavior with a reasonable accuracy. The simplified OWT model does not capture the higher-order structural modes involving blade deformation; these modes are more important for response dynamics of the blades.

6.2. Effect of the aerodynamic damping

To investigate the effect of the aerodynamic damping on the collision results, the comparisons between cases 1–9 and cases 10–18 are made.

Figs. 7–9 show the comparison of displacement histories of the tower-top node in the x-direction (Fig. 1) for different wind directions and different wind speeds. Fig. 7 shows that the tower-top displacement increases slowly and reaches a steady state during the first 10 s which is induced by the wind load acting in the x-direction. In contrast, when the wind direction is 90°, the tower-top displacement is small prior to the impact due to the small wind load in the x-direction, as shown in Fig. 8. Comparing Figs. 7 and 9, we see that the magnitudes of tower-top displacement are similar when the wind velocity has constant magnitude but with opposite directions. The ship impact occurs around 10 s and its duration is approximately 1.44 s. After the impact, there is no difference between cases 2, 5, 8 and cases 11, 14, 17 when the impact velocity is perpendicular to the wind speed (Fig. 8). On the contrary, the simulations with consideration of aerodynamic damping yield much smaller amplitude of the tower vibration when the impact velocity has the same or opposite directions of the wind velocity (Figs. 7 and 9). This observation indicates that the aerodynamic damping has a significant effect on the tower-top motion when wind directions are parallel to the ship impact velocity. In addition, this difference is the greatest when the wind speed is 11.4 m/s (see Figs. 7 (c) and Fig. 9 (c)), as the aerodynamic damping for this case is the largest. From Figs. 7–9, it is also seen that the period of the tower oscillation after the impact is approximately 4.4 s, which is close to the first eigen period of the OWT (4.2 s).

The maximum resultant tower-top displacements for a wind speed of 11.4 m/s are compared in Table 4. It is clearly shown that the discrepancy is largest when the impact velocity has opposite direction of the wind velocity. The maximum resultant tower-top displacement reaches 2.39 m when the aerodynamic damping is

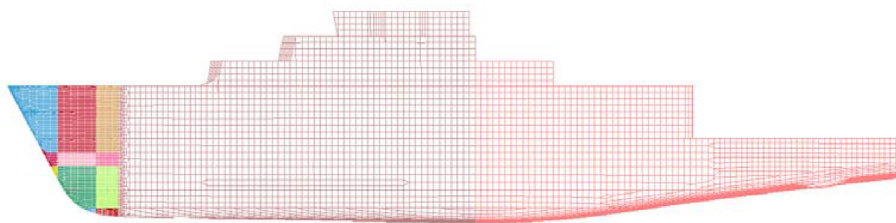


Fig. 5. Finite element model of the ship.



Fig. 6. Finite element model of the OWT.

Table 2
Material parameters of the deformable bow and the OWT.

Material property	Deformable ship bow	OWT
Density ρ (kg/m ³)	7850	8500
Young's modulus E (GPa)	207	207
Poisson's ratio ν (-)	0.3	0.3
Yield stress σ_y (MPa)	275	355
Strength coefficient k (MPa)	740	760
Hardening exponent n (-)	0.24	0.225
Plastic failure strain ϵ_f (-)	0.3	0.3

considered and the wind direction is 0°. This maximum is greater than those of the wind direction of 90° or 180°. Accordingly, the relative direction between the wind speed and the impact velocity also has an influence on the maximum tower-top displacement. Large tower-top displacement may arise when the impact velocity and the wind speed are collinear.

The internal energy histories of the OWT for a wind speed of 11.4 m/s are compared in Figs. 10–12. During the first 10 s, the values of internal energy for these cases are the same, as the internal energy is governed by the wind loads. Around 10 s, the energy dissipation increases rapidly due to the ship impact. There are obvious fluctuations after the impact, and the peaks and valleys of the internal energy are in good correspondence with those of the tower-top displacement (Figs. 7–9). This is because the flexibility of

the soil is taken into account in the simulations and the OWT oscillates after the ship impact. Except for the wind direction of 90°, the peak values of the internal energy are much smaller when the aerodynamic damping is considered, which means that the aerodynamic damping significantly affects the elastic energy stored in the tower structure. On the other hand, the energy dissipated through plastic deformation of the crushed OWT is on the same level. Overall, consideration of the aerodynamic damping is more important for elastic deformation than for plastic deformation of the OWT.

The comparisons of maximum local indentation, maximum contact force and maximum resultant tower-top acceleration for a wind speed of 11.4 m/s are presented in Table 5. It is observed that the aerodynamic damping has a limited influence on these response variables. This can be explained by the fact that the collision duration, i.e., 1.44 s, is so short that the effect of the aerodynamic damping is limited during the collision phase. The maximum allowable acceleration of the nacelle is 6 m/s² according to Siemens Gamesa [38]. As shown in Table 5, the maximum resultant accelerations for these cases are approximate 5 m/s², which are below the maximum allowable acceleration and hence not critical to the drivetrain components. The maximum local indentation values for these cases are less than 0.2 m, which indicates that no major repairs are required for the OWT under the considered ship impact. The relatively small local indentation can be explained by the selected impact location, which is 1.75 m below the connection between the tower and the transition piece. For this impact location, the tower wall is thick and the structural stiffness is large.

6.3. Effect of the impact velocity

To investigate the effect of the impact velocity, we vary the velocity from 1 m/s to 3 m/s for different ship-OWT collision cases in which the mean wind speed is fixed as 11.4 m/s (rated speed) and the corresponding aerodynamic damping is taken into account; see cases 16–24 in Table 3.

Table 6 presents the maximum resultant tower-top displacement for these cases. When the ship impacts the OWT at 1 m/s, the tower-top displacement does not exceed 2.5 m. When the ship has a impact velocity of 2 m/s, the tower-top displacement grows to 3.16 m for a wind direction of 180°, whereas the OWT collapses for wind directions of 0° and 90°. The collapse of the OWT for a wind direction of 180° occurs at an impact velocity of 3 m/s.

Fig. 13 shows collapses of the OWT under different wind directions. It can be observed that the collapse direction of and location on the tower are different. The tower falls into the sea in the same impact direction for a wind direction of 0° and at an angle of approximately 44° relative to the impact direction for a wind direction of 90°. In contrast, for a wind direction of 180°, the tower tilts toward the ship and collapses, followed by the nacelle falling onto the deck. This scenario can be regarded as the most dangerous case. Therefore, a high ship impact velocity opposite to the wind direction should always be avoided in an accident, considering the

Table 3
Summary of the load cases considered in the study.

Load case	Ship bow	Ship velocity [m/s]	Wind speed [m/s]	Turbine condition	Aerodynamic damping [kNs/m]	Wind direction (°)
1	Rigid	1	5	Operating	0	0
2	Rigid	1	5	Operating	0	90
3	Rigid	1	5	Operating	0	180
4	Rigid	1	25	Operating	0	0
5	Rigid	1	25	Operating	0	90
6	Rigid	1	25	Operating	0	180
7	Rigid	1	11.4	Operating	0	0
8	Rigid	1	11.4	Operating	0	90
9	Rigid	1	11.4	Operating	0	180
10	Rigid	1	5	Operating	51.5	0
11	Rigid	1	5	Operating	51.5	90
12	Rigid	1	5	Operating	51.5	180
13	Rigid	1	25	Operating	67.7	0
14	Rigid	1	25	Operating	67.7	90
15	Rigid	1	25	Operating	67.7	180
16	Rigid	1	11.4	Operating	90.4	0
17	Rigid	1	11.4	Operating	90.4	90
18	Rigid	1	11.4	Operating	90.4	180
19	Rigid	2	11.4	Operating	90.4	0
20	Rigid	2	11.4	Operating	90.4	90
21	Rigid	2	11.4	Operating	90.4	180
22	Rigid	3	11.4	Operating	90.4	0
23	Rigid	3	11.4	Operating	90.4	90
24	Rigid	3	11.4	Operating	90.4	180
25	Rigid	1	0	Parked	0	0
26	Rigid	1	3	Parked	0	0
27	Rigid	1	8	Operating	66.6	0
28	Rigid	1	14	Operating	82	0
29	Rigid	1	17	Operating	75.7	0
30	Rigid	1	20	Operating	67.7	0
31	Rigid	1	23	Operating	60.4	0
32	Rigid	1	28	Parked	0	0
33	Rigid	1	30	Parked	0	0
34	Deformable	1	11.4	Operating	90.4	0
35	Deformable	2	11.4	Operating	90.4	0
36	Deformable	3	11.4	Operating	90.4	0

collapse direction of the OWT tower. The collapse location is at 15 m above the connection between the tower and the transition piece for wind directions of 0° and 90°. Near the collapse location, the tower has a thickness of 24.5 mm. For a wind direction of 180°, the collapse location is approximately 35 m above the connection and the tower has a thickness of 23.4 mm in that region. This difference is due to the different impact velocities. Besides, it can be observed that the collapse of the tower is induced by structural buckling under the wind loads after the ship impact, which indicates that the stability of the OWT has reduced due to local impact.

6.4. Effect of the mean wind speed

The actual wind condition is turbulent, but for collision simulations, the aerodynamic forces in the first few seconds after the impact will play a key role, and thus we only consider various mean wind speeds for the analysis. If we consider turbulent wind, Monte Carlo simulations with random seeds should be used which is computationally expensive for such analyses. Therefore, twelve simulations are carried out in which the mean wind speed varies from 0 m/s to 30 m/s for a wind direction of 0°, and an impact velocity of 1 m/s is selected; see cases 10, 13, 16 and cases 25–33. The aerodynamic damping are taken into account in these cases, and the corresponding values and the status of the wind turbine for different mean wind speeds are presented in Table 3.

Fig. 14 shows the maximum resultant tower-top displacement for a range of wind speeds. It can be observed that the maximum resultant tower-top displacement initially rises along with the

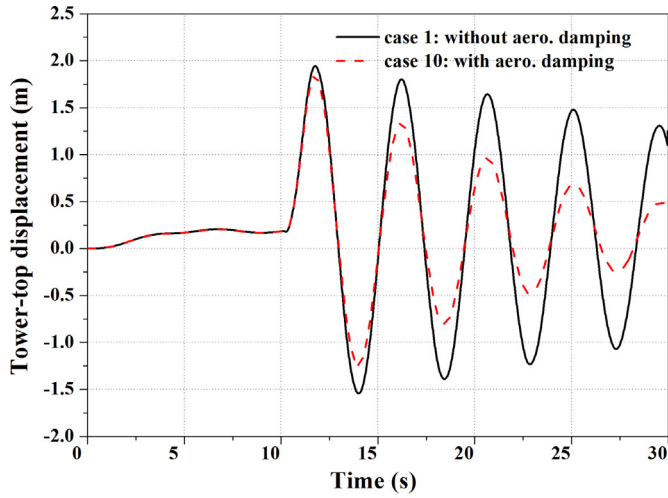
increase of wind speed and the highest value is attained when the mean wind speed is close to the rated (11.4 m/s), and then the maximum tower-top displacement slowly decreases with the increase of wind speed until the wind speed reaches 25 m/s. For wind speeds above 25 m/s, the maximum tower-top displacement increases rapidly due to a lack of aerodynamic damping. It can be concluded that the wind speed has a major influence on the tower-top displacement. The maximum value of tower-top displacement is 2.39 m for a mean wind speed of 11.4 m/s, which is approximately 1.4 times than that obtained without considering wind loads. This indicates that ignoring the wind loads may underestimate the maximum tower-top displacement.

6.5. Collision of a deformable bow with the OWT

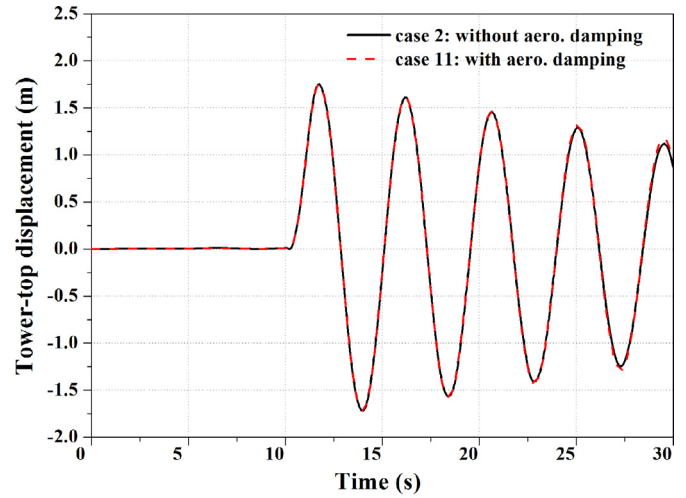
In reality, the striking ship and the OWT structures deform simultaneously during a collision. It is conservative for the OWT to assume that the service vessel is rigid and the total energy is only transferred to the OWT's support structure. Therefore, a deformable bow is considered in addition. The wind loads and the aerodynamic damping for the mean wind speed of 11.4 m/s are considered. The impact velocity is assumed to follow the wind direction (cases 34–36).

6.5.1. Comparison with numerical results of the rigid bow

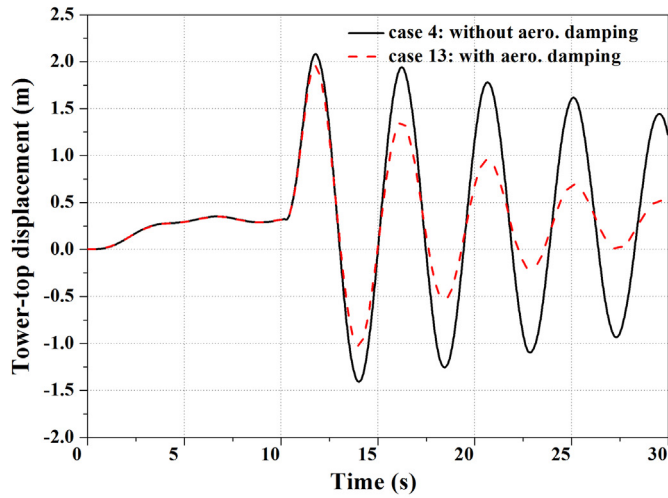
Fig. 15 shows the contact force histories obtained by the numerical method considering both the rigid bow and the deformable bow when the impact velocity is 1 m/s. It can be observed that the maximum force is 7.67 MN when the striking ship has a deformable



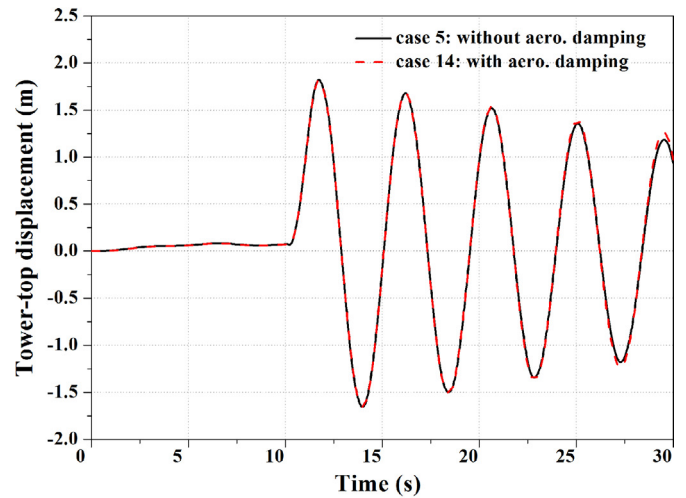
(a) Wind speed of 5 m/s



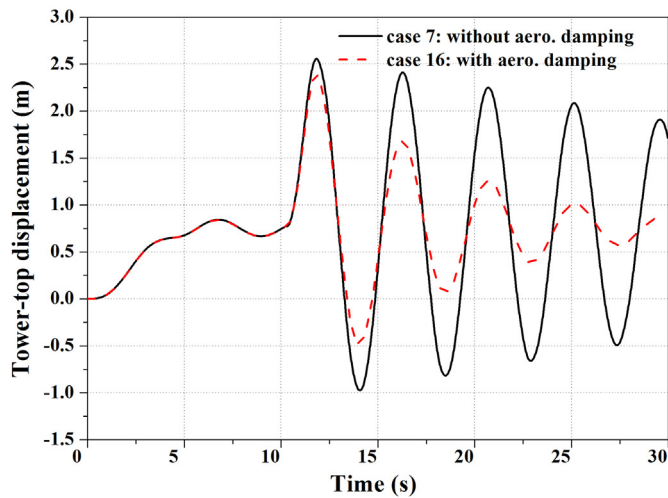
(a) Wind speed of 5 m/s



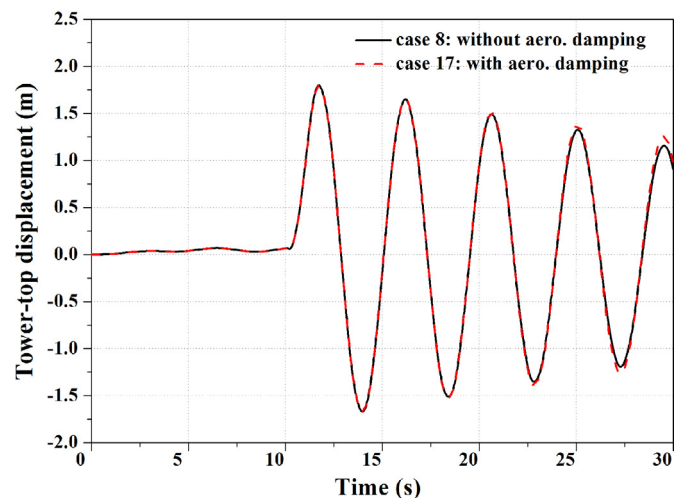
(b) Wind speed of 25 m/s



(b) Wind speed of 25 m/s



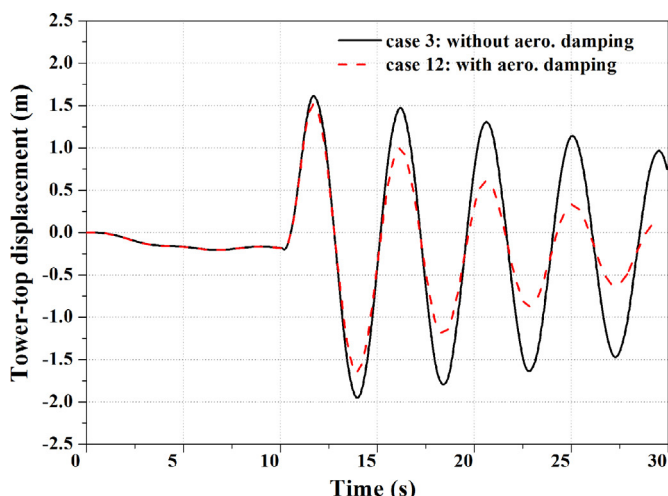
(c) Wind speed of 11.4 m/s



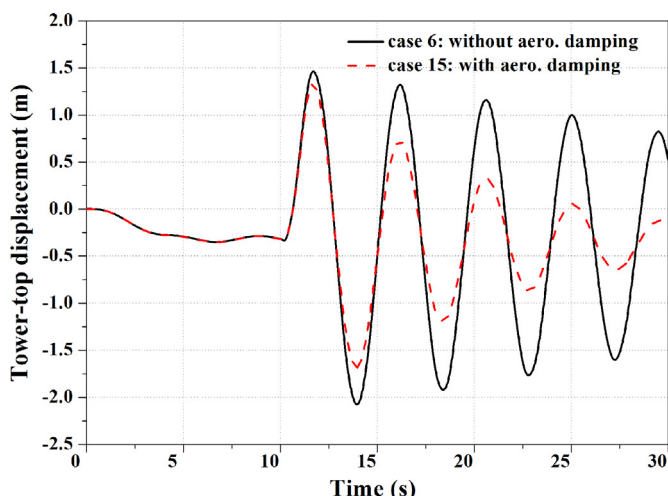
(c) Wind speed of 11.4 m/s

Fig. 7. Comparison of the tower-top displacement in the x-direction for a wind direction of 0°.

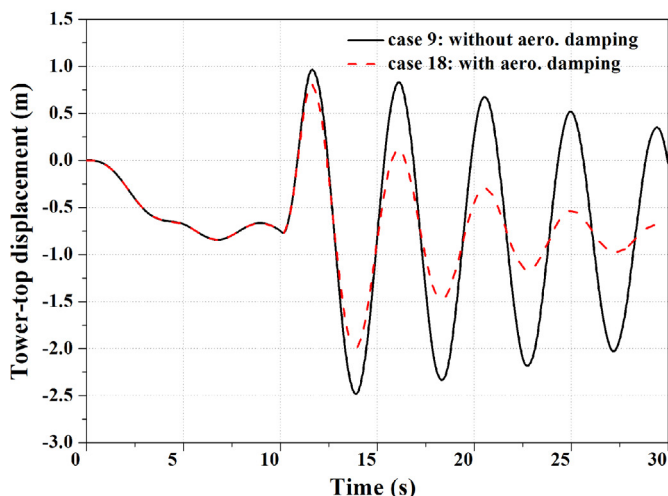
Fig. 8. Comparison of the tower-top displacement in the x-direction for a wind direction of 90°.



(a) Wind speed of 5 m/s



(b) Wind speed of 25 m/s



(c) Wind speed of 11.4 m/s

Fig. 9. Comparison of the tower-top displacement in the x-direction for a wind direction of.

bow, much lower than the force (9.67 MN) when the striking ship is rigid. As shown by the red dashed line, the contact force has a longer duration and undergoes more fluctuations for the deformable bow. In addition, the maximum resultant tower-top displacement and maximum local indentation are 1.92 m and 0.098 m, respectively, which are much smaller than the results (2.39 m and 0.17 m) of the rigid-bow simulations.

The temporal variation of the internal energy absorbed by the OWT and the deformable bow is plotted in Fig. 16, and the internal energy of the OWT obtained under the rigid bow impact is also given. It is seen that the total internal energy absorbed by the ship is 1.6 MJ, which is approximate 56% of the impact energy ($\frac{1}{2}mV_{ship}^2 = 2.88$ MJ). When the OWT is impacted by the deformable bow, the maximum internal energy absorbed by the OWT is 1.96 MJ, which is 44% less than that of the simulation with the rigid bow (3.50 MJ). In addition, for the case with the deformable bow, the energy absorbed by the plastic deformation is less, which agrees with the smaller local indentation observed.

6.5.2. Comparison with the analytical results

The simplified analytical method is applied to cases 34–36. According to Refs. [39,40], the damping ratios for the structural damping, radiation damping, soil damping can be set to 1%, 0.07% and 0.36%, respectively. The aerodynamic damping (90.4 kN·s/m) calculated by the HAWC2 code is used.

The comparison results between the numerical and analytical methods for different impact velocities are presented in Figs. 17–19. It can be seen that the trends agree very well of the numerical and analytical results including the maximum tower-top displacement, the maximum contact force and the total energy dissipation of the ship. These variables increase with an increasing impact velocity. These values are also presented in Tables 7–9 where the discrepancies are measured in percentage using the numerical results as the references.

For an impact velocity of 3 m/s, the collapse of the OWT occurs due to structural buckling when the tower-top displacement reaches 4.65 m; see the red cross marked in Fig. 17. The analytical method has a limitation and cannot evaluate the collapse of the tower. Except for the tower-top displacement, the results obtained by the analytical method agree well with those obtained by the numerical method for this case. When the ship impacts the OWT at 1 m/s, the analytical results are also close to the numerical results, especially for the maximum contact force. While for an impact velocity of 2 m/s, the discrepancy of the maximum contact force between the two methods is greatest (55%). This observation is aligned with the comparison result of the energy dissipated by the ship. During an actual collision, the ship absorbs much more plastic energy, which yields lower maximum contact force and smaller maximum tower-top displacement than the analytical results. In addition, the differences between the numerical and analytical results are mainly due to the assumptions made in the analytical method especially related to the boundary conditions. Still, the estimation obtained by the simplified analytical approach is acceptable for impact velocities of 1 m/s and 3 m/s.

The present analytical approach with consideration of the damping effect is developed on the basis of Pedersen’s analytical method. As the damping effect can be neglected during the first crushing phase, there is no difference in both the maximum contact force and the energy dissipated by the ship between the two analytical methods. The discrepancies of the maximum tower-top displacement between the two analytical and numerical results are presented in Table 10. It is observed that the discrepancy between the present analytical and numerical results is smaller, which indicates that the presented analytical approach gives a

Table 4
Comparison of the maximum resultant tower-top displacement for a wind speed of 11.4 m/s.

Wind direction [o]	Maximum resultant tower-top displacement [m]		Discrepancy [%]
	Without aerodynamic damping	With aerodynamic damping	
0	2.56	2.39	7
90	1.91	1.91	0
180	2.48	2	24

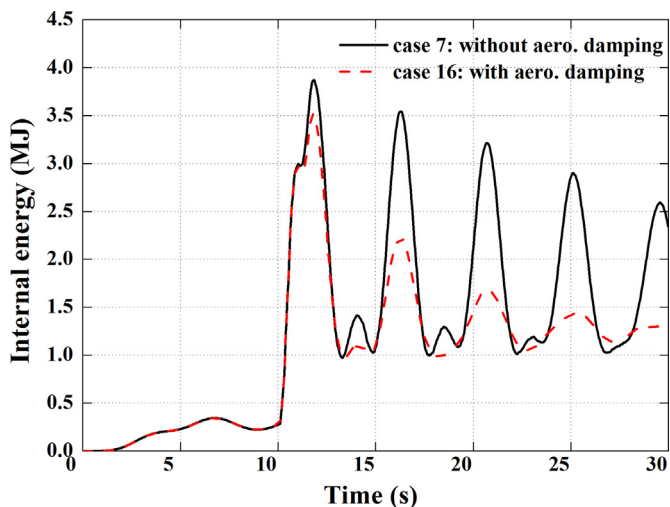


Fig. 10. Comparison of internal energy for a wind direction of 0°.

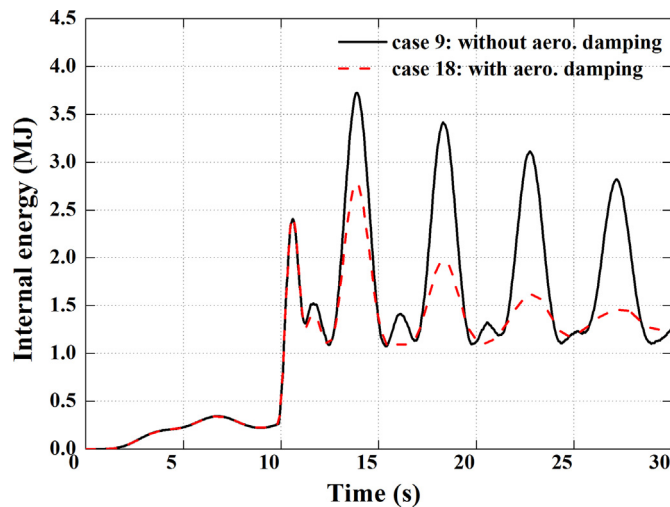


Fig. 12. Comparison of internal energy for a wind direction of 180°.

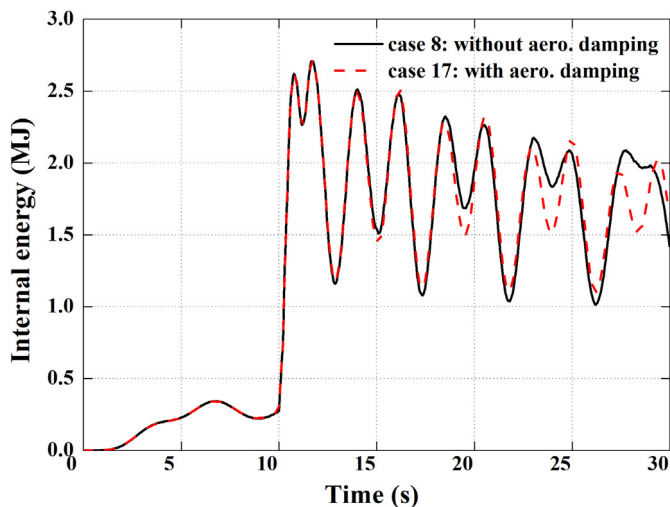


Fig. 11. Comparison of internal energy for a wind direction of 90°.

more accurate estimation with respect to the maximum tower-top displacement compared to Pedersen’s analytical method.

Fig. 20 shows the plastic strain contour images of the impacted transition piece for different impact velocities. It is observed that both the damage area and maximum plastic strain increase along with the impact velocity. The maximum strain for the impact velocity of 3 m/s is approximately 0.1, which is smaller than the corresponding failure strain. This reveals that failure does not occur near the ship impact area.

7. Conclusions

In this paper, both numerical and analytical methods are used to investigate the collision between a ship and a monopile-supported offshore wind turbine, and the interaction between the wind loads and the tower-top motion is taken into account. Depending on the wind direction, wind speed, aerodynamic damping, impact velocity and ship bow rigidity, 36 collision cases in total are simulated and analyzed.

The major findings when the rigid bow is used are as follows:

- The aerodynamic damping has a limited effect on the tower response for a wind direction of 90°. However, for wind directions of 0° and 180°, the amplitude of the tower vibration and the corresponding elastic energy absorbed by the offshore wind turbine are much smaller when the aerodynamic damping is considered.
- The impact velocity and the wind direction significantly affect the wind turbine response. For wind directions of 0° and 90°, the tower falls into the sea at an impact velocity of 2 m/s. The tower falls onto the ship at an impact velocity of 3 m/s for a wind direction of 180°, which can be regarded as the most dangerous case due to the second impact between the nacelle and the ship deck. The collapse of the wind turbine tower is due to structural buckling under the combined load effects of ship impact, wind loads, and the tower-top gravity.
- The tower-top displacement is influenced by the mean wind speed. The maximum tower-top displacement is largest for a mean wind speed of 11.4 m/s. Ignoring the wind loads may underestimate the tower response.

The comparison between the numerical results obtained by the rigid bow and the deformable bow is made. The deformable bow

Table 5
Results for cases 7–9 and 16–18.

Wind direction [°]	Considering aerodynamic damping	Maximum local indentation (m)	Maximum contact force (MN)	Maximum tower-top acceleration (m/s ²)
0	no	0.17	9.66	5.01
	yes	0.17	9.67	4.70
90	no	0.19	9.82	4.87
	yes	0.19	9.82	4.92
180	no	0.18	9.85	5.06
	yes	0.18	9.85	4.84

Table 6
Maximum resultant tower-top displacement for cases 16–24.

Wind direction [°]	Maximum resultant tower-top displacement [m]		
	velocity of 1 m/s	velocity of 2 m/s	velocity of 3 m/s
0	2.39	collapse	collapse
90	1.91	collapse	collapse
180	2.00	3.16	collapse

yields lower maximum contact force, smaller local indentation and less energy dissipated by the offshore wind turbine, and the force obtained by the deformable bow has a longer duration and more fluctuations.

A simplified analytical method is extended and applied to predict the maximum tower-top displacement, the maximum contact

force and the total energy dissipated by the ship, and compared to the numerical results obtained by the deformable bow. The comparison shows that the analytical method can give an acceptable estimation for impact velocities of 1 m/s and 3 m/s. Still, the analytical method cannot evaluate the collapse of the offshore wind turbine and the accuracy is relatively low for an impact velocity of 2 m/s.

The scope of this work is limited. The presence of wave forces will affect the monopile vibrations, which are ignored in the presented work. Consideration of the hydrodynamic loads on the monopile foundation during the analysis of ship-wind turbine collision will be addressed in the future. Further, an extension of the analytical work to floating wind turbines can be considered.

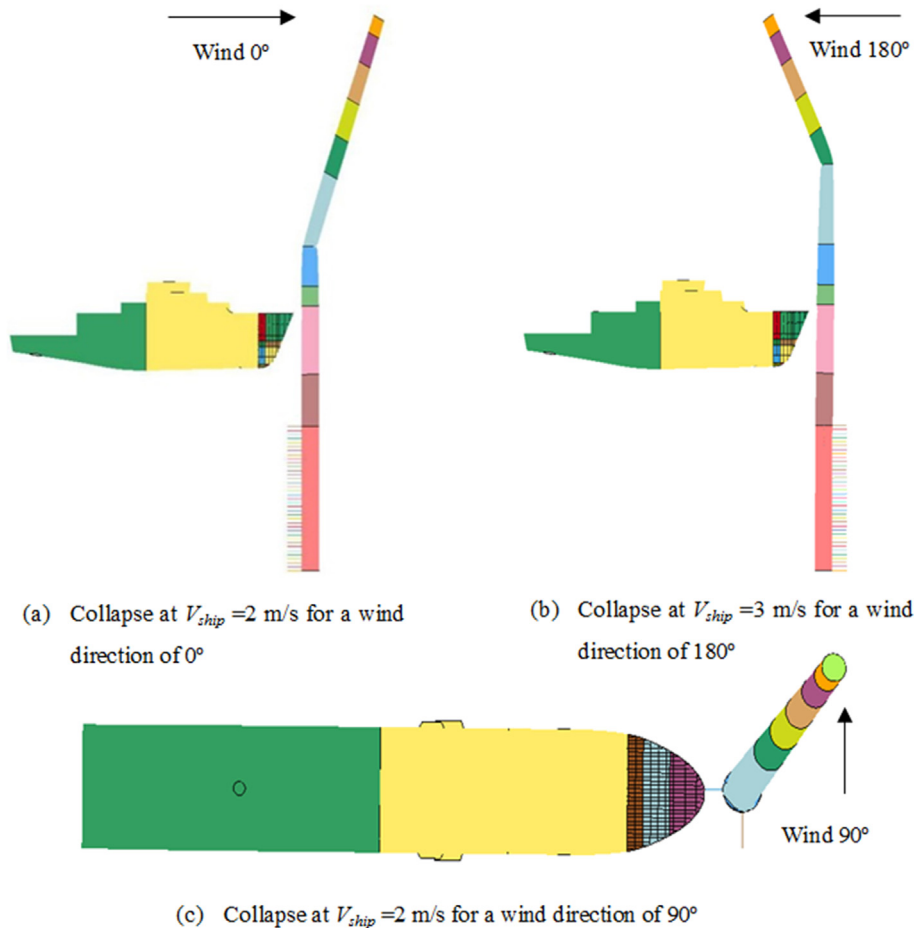


Fig. 13. Collapse of the OWT: (a) case 19; (b) case 24; (c) case 20.

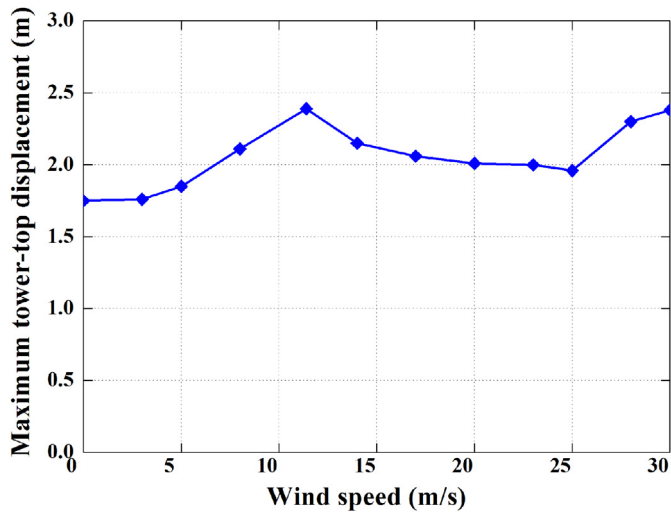


Fig. 14. Maximum resultant tower-top displacement for different mean wind speeds.

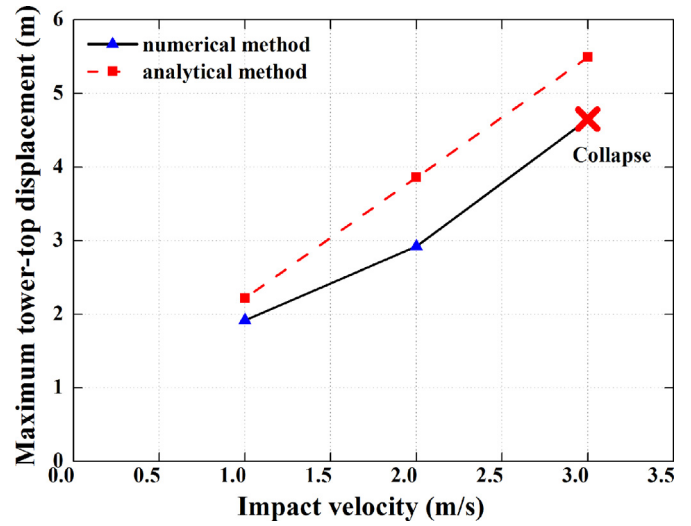


Fig. 17. Comparison of the maximum tower-top displacement.

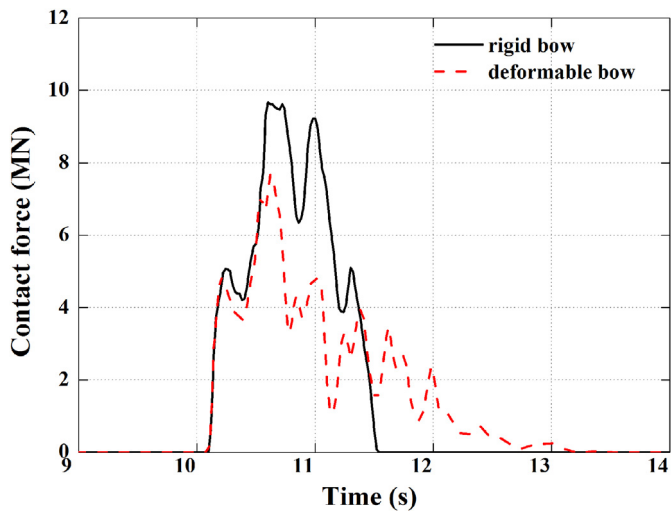


Fig. 15. Comparison of contact force history ($V_{ship} = 1$ m/s).

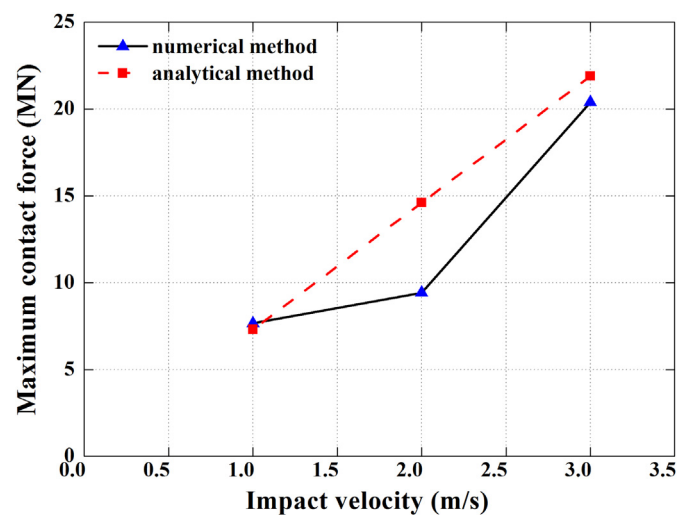


Fig. 18. Comparison of the maximum contact force.

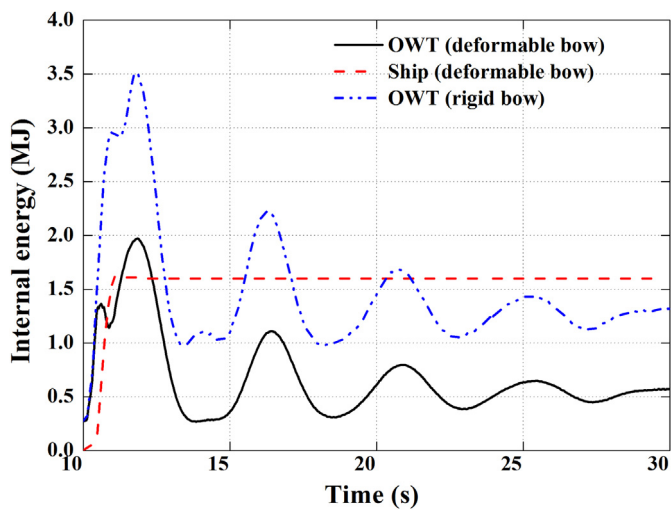


Fig. 16. Comparison of internal energy history ($V_{ship} = 1$ m/s).

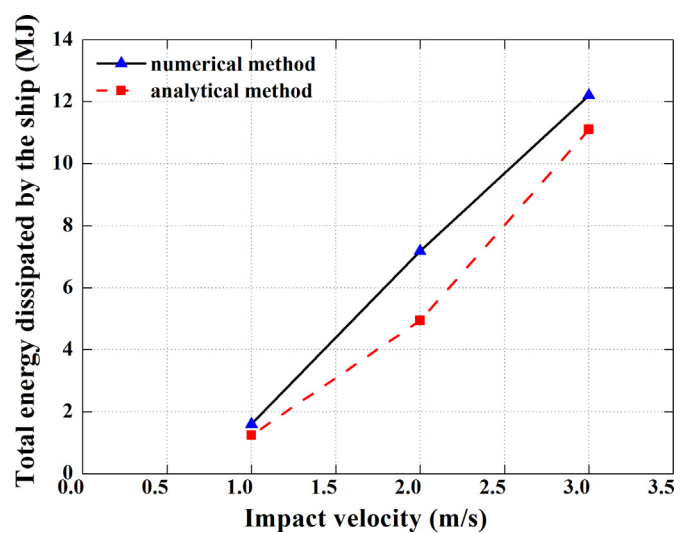


Fig. 19. Comparison of the total energy dissipated by the ship.

Table 7
Comparison results for an impact velocity of 1 m/s.

Method	Maximum tower-top displacement [m]	Maximum contact force [MN]	Energy dissipated by the ship [MJ]
Numerical	1.92	7.67	1.6
Analytical	2.22	7.3	1.24
Discrepancy	16%	5%	23%

Table 8
Comparison results for an impact velocity of 2 m/s.

Method	Maximum tower-top displacement [m]	Maximum contact force [MN]	Energy dissipated by the ship [MJ]
Numerical	2.92	9.42	7.18
Analytical	3.86	14.6	4.94
Discrepancy	32%	55%	31%

Table 9
Comparison results for an impact velocity of 3 m/s.

Method	Maximum tower-top displacement [m]	Maximum contact force [MN]	Energy dissipated by the ship [MJ]
Numerical	4.65-collapse	20.4	12.2
Analytical	5.49	21.9	11.1
Discrepancy	18%	7%	9%

Table 10
The discrepancies of the maximum tower-top displacement between the two analytical and numerical results for different impact velocities.

Impact velocity [m/s]	Discrepancy between Pedersen’s analytical and numerical results [%]	Discrepancy between the present analytical and numerical results [%]
1	20	16
2	37	32
3	23	18

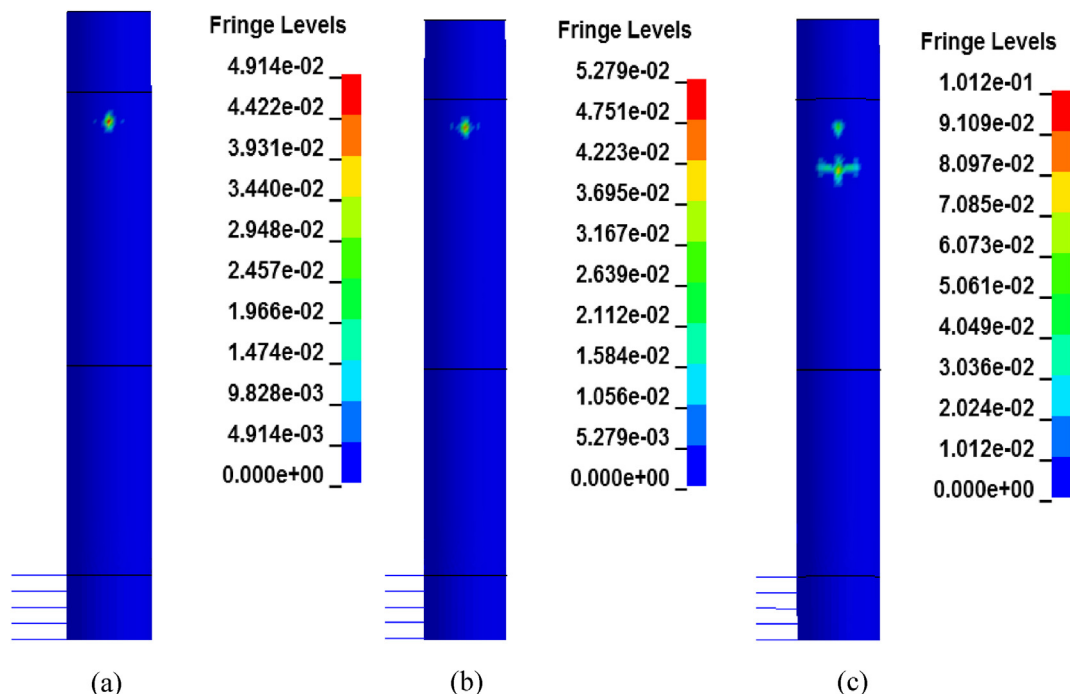


Fig. 20. Plastic strain of the impacted transition piece: (a) $V_{ship} = 1$ m/s, (b) $V_{ship} = 2$ m/s, (c) $V_{ship} = 3$ m/s.

Author contributions

The authors (Ming Song, Zhiyu Jiang and Wei Yuan) declare that they all have contributed significantly to the article. Specifically, Ming Song contributed to numerical simulation and development of analytical methods, and writing; Zhiyu Jiang contributed to concept construction, numerical modeling, results discussion, and writing; Wei Yuan contributed to numerical modeling and analysis.

Declaration of competing interest

The authors declare that they have no known competing financial interests or personal relationships that could have appeared to influence the work reported in this paper.

Acknowledgements

This work has been financially supported by the Natural Science Foundation of Jiangsu Province of China, grant number BK20200998. The first author also acknowledges the visiting scholar scholarship provided by University of Agder, Norway.

References

- [1] Global Wind Energy Council (GWEC), Global Wind Report - Annual Market Update, 2017. <http://gwec.net/publications/global-wind-report-2/>.
- [2] Pineda P. Tardieu, The European Offshore Wind Industry Key Trends and Statistics, 2016. <https://windeurope.org/about-wind/statistics/offshore/european-offshore-wind-industry-key-trends-and-statistics-2016/>.
- [3] Z. Jiang, W. Hu, W. Dong, Z. Gao, Z. Ren, Structural reliability analysis of wind turbines: a review, *Energies* 10 (12) (2017) 2099.
- [4] K.O. Ronold, G.C. Larsen, Reliability-based design of wind-turbine rotor blades against failure in ultimate loading, *Eng. Struct.* 22 (6) (2000) 565–574.
- [5] N.J. Tarp-Johansen, Partial safety factors and characteristic values for combined extreme wind and wave load effects, *J. Sol. Energy Eng.* 127 (2) (2005) 242–252.
- [6] Z. Jiang, M. Karimirad, T. Moan, Dynamic response analysis of wind turbines under blade pitch system fault, grid loss, and shutdown events, *Wind Energy* 17 (9) (2014) 1385–1409.
- [7] L. Dai, S. Ehlers, M. Rausand, I.B. Utne, Risk of collision between service vessels and offshore wind turbines, *Reliab. Eng. Syst. Saf.* 109 (2013) 18–31.
- [8] NORSOK, N-004: Design of Steel Structures. Annex A: Design against Accidental Actions, 2004.
- [9] BSH, Design of Offshore Wind Turbines, Hamburg and Rostock, 2007.
- [10] International Electrotechnical Commission, IEC 61400-3. Wind Turbines- Part 3: Design Requirements for Offshore Wind Turbines, IEC, Geneva, Switzerland, 2009.
- [11] DNVGL-ST-0437. Loads and Site Conditions for Wind Turbines 2016.
- [12] L. Buldgen, H. Le Sourne, T. Pire, Extension of the super-elements method to the analysis of a jacket impacted by a ship, *Mar. Struct.* 38 (2014) 44–71.
- [13] T. Pire, H. Le Sourne, S. Echeverry, P. Rigo, Analytical formulations to assess the energy dissipated at the base of an offshore wind turbine jacket impacted by a ship, *Mar. Struct.* 59 (2018) 192–218.
- [14] P.T. Pedersen, J.J. Jensen, Ship impact analysis for bottom supported offshore structures, in: *Advances in Marine Structures II*, Elsevier Applied Science, 1991, pp. 276–295.
- [15] P.T. Pedersen, S. Zhang, Impact mechanics of ship collisions, *Mar. Struct.* 11 (1998) 429–449.
- [16] P.T. Pedersen, Ship collisions against wind turbines, quays and bridge piers, in: *Proceedings of the 6th International Conference on Collision and Grounding of Ships and Offshore Structures*, ICCGS, 2013, pp. 273–280.
- [17] J. Amdahl, T. Holmas, High Energy Ship Collisions with Jacket Supported Offshore Wind Turbines, *Proceedings of the International Conference on Computational Methods in Marine Engineering*, Barcelona, Spain, 2011.
- [18] A. Bela, H. Le Sourne, L. Buldgen, P. Rigo, Numerical crashworthiness analysis of an offshore wind turbine monopile impacted by a ship, in: *MARSTRUCT 2015 5th International Conference on Marine Structures*, Taylor & Francis Group, 2015.
- [19] H. Le Sourne, A. Barrera, J.B. Maliakel, Numerical crashworthiness analysis of an offshore wind turbine jacket impacted by a ship, *J. Mar. Sci. Technol.* 23 (5) (2015) 694–704.
- [20] H.F. Ramberg, High Energy Ship Collisions with Bottom Supported Offshore Wind Turbines, M.S. Thesis, Norwegian University of Science and Technology, 2011.
- [21] D. Moulas, M. Shafiee, A. Mehmanparast, Damage analysis of ship collisions with offshore wind turbine foundations, *Ocean. Eng.* 143 (2017) 149–162.
- [22] E. Hao, C. Liu, Evaluation and comparison of anti-impact performance to offshore wind turbine foundations: monopile, tripod, and jacket, *Ocean. Eng.* 130 (2017) 218–227.
- [23] A. Bela, H. Le Sourne, L. Buldgen, P. Rigo, Ship collision analysis on offshore wind turbine monopile foundations, *Mar. Struct.* 51 (2017) 220–241.
- [24] J.O. Hallquist, LS-DYNA User's Manuals Version 971, vols. 1 & 2, 2013.
- [25] M.S.C. Patran, Patran User's Guide, 2012.
- [26] N.N. Sørensen, General Purpose Flow Solver Applied to Flow over Hills, vol. 827, Risø National Laboratory, Roskilde, 1995.
- [27] H. Glauert, in: W.F. Durand (Ed.), *Airplane Propellers. Aerodynamic Theory Chapter vol. II*, Dover Publication Inc., New York, 1935, pp. 251–268.
- [28] J.M. Jonkman, M.L. Buhl Jr., FAST User's Guide, Tech. rep. NREL/EL-500-38230, National Renewable Energy Laboratory, 2005.
- [29] T.J. Larsen, A.M. Hansen, How 2 HAWC2, the user's manual, Risø-R-1597 (2018).
- [30] D.C. Salzmann, J. Van der Tempel, Aerodynamic Damping in the Design of Support Structures for Offshore Wind Turbines, *Proceedings of the Copenhagen Offshore Wind Conference*, Delft, The Netherlands, 2005, pp. 26–28.
- [31] M.J. Kühn, Dynamics and Design Optimisation of Offshore Wind Energy Conversion Systems, DUWIND, Delft University Wind Energy Research Institute, 2001.
- [32] J. Van Der Tempel, Design of Support Structures for Offshore Wind Turbines, PhD Thesis, TU Delft, The Netherlands, 2006.
- [33] J.M. Hegseth, E.E. Bachynski, A semi-analytical frequency domain model for efficient design evaluation of spar floating wind turbines, *Mar. Struct.* 64 (2019) 186–210.
- [34] E.E. Bachynski, Design and Dynamic Analysis of Tension Leg Platform Wind Turbines, PhD thesis, Norwegian University of Science and Technology, 2014.
- [35] S.P. Lin, Analysis on deflection formula of steel tube pole with variable cross-section, *Special Structures* 29 (6) (2012) 26–29.
- [36] J. Jonkman, S. Butterfield, P. Passon, T. Larsen, T. Camp, J. Nichols, J. Azcona, A. Martinez, Offshore Code Comparison Collaboration within IEA Wind Annex XXIII: Phase II Results, IEA European Offshore Wind Conference, Berlin, Germany, December, 2007, pp. 4–6.
- [37] H.S. Alsos, J. Amdahl, On the resistance of tanker bottom structures during stranding, *Mar. Struct.* 20 (4) (2007) 218–237.
- [38] C.G. Liu, E.T. Hao, S.B. Zhang, Optimization and application of a crashworthy device for the monopile offshore wind turbine against ship impact, *Appl. Ocean Res.* 51 (2015) 129–137.
- [39] J. Jonkman, S. Butterfield, W. Musial, G. Scott, Definition of a 5-MW Reference Wind Turbine for Offshore System Development, Tech. rep. NREL/TP-500-38060, National Renewable Energy Laboratory, February 2009.
- [40] R. Shirzadeh, C. Devriendt, M.A. Bidakhvidi, P. Guillaume, Experimental and computational damping estimation of an offshore wind turbine on a monopile foundation, *J. Wind Eng. Ind. Aerod.* 120 (2013) 96–106.